

Symbolic Dynamics from Homoclinic Tangles

Pieter Collins

Department of Mathematical Sciences

University of Liverpool

Liverpool L69 7ZL, U.K.

pcollins@liv.ac.uk

4 May 2001

Abstract

We give a method for finding symbolic dynamics for a planar diffeomorphism with a homoclinic tangle. The method only requires a finite piece of tangle, which can be computed with available numerical techniques. The symbol space is naturally given by components of the complement of the stable and unstable manifolds. The shift map defining the dynamics is a factor of a subshift of finite type, and is obtained from a graph related to the tangle. The entropy of this shift map is a lower bound for the topological entropy of the planar diffeomorphism. We give examples arising from the Hénon family.

Keywords: Homoclinic tangle, symbolic dynamics, topological entropy, Hénon map.

1 Introduction

Chaotic behaviour in deterministic systems was first highlighted in Poincaré's treatise *New Methods of Celestial Mechanics*. In this work, he discovered that the stable and unstable sets of a fixed point of a dynamical system could form an extremely complicated pattern, now known as a *homoclinic tangle*, with infinitely many intersections of the two sets. The existence of a homoclinic tangle in the three-body problem proved the non-integrability of this system. Since then, there has been a great deal of interest in the properties of homoclinic tangles and their effects on the dynamics of a system. The most important result is that a system with a homoclinic tangle must be chaotic and have positive topological entropy. Most existing theory deals with local behaviour near the tangle, though many other types of behaviour have been conjectured from numerical evidence. A good exposition of many of the most important results is given by Palis and Takens [1993].

The purpose of this paper is to show how to obtain global information about the dynamics of a planar diffeomorphism with a homoclinic tangle. The methods given here are directly applicable to forced oscillators and other three-dimensional flows with well-defined Poincaré return maps. We present an algorithm for computing symbolic dynamics and a lower estimate for the topological entropy of the diffeomorphism. The concepts and

procedures used are illustrated in detail with examples from the Hénon family, which is likely to be familiar to readers. Results have also been obtained for the Duffing equation [Collins, 1999b].

There are a number of features of this method which make it particularly suitable for use in applications:

- We need only consider finite pieces of stable and unstable manifold. We call the resulting subset of the homoclinic tangle a *trellis*. Trellises can be computed using existing algorithms, and since they only have finitely many intersections, the topology of the trellis can be found using basic techniques of computational geometry.
- The algorithms used are all highly amenable to automation, and the author is currently working on a computer implementation.
- The *regions* of phase space determined by the trellis give a natural way of describing orbits symbolically.
- The symbolic dynamics typically gives information about the transients of the system which are often hard to study.
- We obtain a lower bound for the topological entropy of the system, which measures the degree of chaos. This entropy bound can be shown to be optimal in an appropriate sense, and in some cases can be realized by a structurally stable diffeomorphism.
- Unless the trellis has tangential intersections of stable and unstable curves, the symbolic dynamics is robust under perturbations.
- No assumptions on the form of the equations governing the system (such as being area-preserving) are needed.
- Aside from the numerical computation of stable and unstable manifolds, all results are mathematically rigorous.

The methods developed here are an addition to the growing range of algebraic topological techniques for the study of the global dynamics of low-dimensional systems. The typical use of these techniques is to show that a certain feature of a system (such as a periodic or homoclinic orbit) *forces* the existence of other orbits. One of the most powerful and useful topological tools is the Conley index [Conley, 1978; Mischaikow, 1997], which has been used to compute symbolic dynamics in the Lorentz system [Mischaikow & Mrozek, 1995] and from an experimental time series [Mischaikow *et. al.*, 1999]. Another important area is the study of the dynamics forced by periodic orbits of surface diffeomorphisms, based on *Nielsen-Thurston theory* [Thurston, 1988]. A practical algorithm for computing the dynamics was found by Bestvina and Handel [1995] and independently by Franks and Misiurewicz [1993], and allowed the theory to be applied to a number of physical problems [Boyland *et. al.*, 2000]. Our methods are based on topological fixed-point theory [Collins, 2001; Jiang, 1983], and use a modification of the Bestvina-Handel algorithm.

The symbolic dynamics forced by tangles arising from a system describing escape from a potential well was previously studied in a number of papers by McRobie and Thompson [1993, 1994]. Assumptions on the existence of orbits were used in these papers, and these assumptions can be verified by the methods given here. The area-preserving case

can be studied using the *topological approximation method* of Rom-Kedar [1994], who obtained symbolic dynamics, entropy bounds and escape time estimates for some families of simple trellises. The methods given here extend those of Rom-Kedar by dropping the area-preserving hypothesis and the assumptions on the geometry of the trellis, yielding a natural and unified approach to the subject.

While in this paper, we only consider planar diffeomorphisms with homoclinic tangles, all techniques given here also to planar diffeomorphisms with heteroclinic tangles, and can be generalised to diffeomorphisms on other surfaces. Similar methods can be used to study dynamics on attractors. Extensions to flows in three dimensions without well-defined Poincaré return maps or to two-degree of freedom Hamiltonian systems may also be possible using the Conley index. Diffeomorphisms of higher-dimensional spaces cannot be studied with the techniques used here. Proofs of the main results of this paper, and details of their generalisations can be found in [Collins, 1999a, 1999b].

There are a number of algorithms for computing stable and unstable manifolds, including [Hobson, 1993; Homburg *et. al.*, 1995; Parker & Chua, 1989; Simo, 1989; You *et. al.*, 1991]. In this paper, all trellises were computed using an implementation in DsTool [Back *et. al.*, 1992] by Osinga of the algorithm of Krauskopf and Osinga [1998], which has the advantage of allowing the arc-length of stable and unstable manifolds to be specified. Due to numerical errors, the topology of the computed trellis may differ from that of the actual trellis for the system. However, the computations tend to have much smaller errors than the numerical analysis would predict, and can be relied upon to give the correct topology unless the stable and unstable curves are extremely close to being tangent. In theory, it is possible to verify that the numerically computed trellis is the same as the actual trellis.

An alternative, but equivalent viewpoint to ours is to consider not homoclinic tangles but homoclinic orbits. These can be computed by an algorithm of Beyn and Kleinkauf [1997], which also allows these orbits to be continued as a parameter is varied. Recent work of Handel [1999] and Hulme [2000] allows symbolic dynamics to be computed from homoclinic orbits using one-dimensional techniques similar to ours, though integrating these algorithms with numerical computations may be harder.

The symbolic description we find gives a first approximation of the orbits, and a subsequent problem is to compute these orbits exactly. High period orbits are extremely difficult to find using traditional methods such as Newton's method, but recently new algorithms for this task have been developed [Davidchack & Lai, 1999], [Schmelcher & Diakonov, 1998]. An algorithm for the Hénon family using a symbolic description of orbits [Hansen, 1995] may be particularly effective if extended to general diffeomorphisms.

When using our method to find symbolic dynamics, the orbits found are typically transients, and so do not describe the limiting dynamics. We can use the same techniques to the restriction of a system to an attractor, but even then cannot be sure that the dynamics found do not merely describe transients in this attractor. Recent work has proved the existence of strange attractors in certain special cases; the current state of knowledge can be found in [Wang & Young, 1999]. However, it remains an open problem as to whether attractors such as the Hénon attractor actually are strange attractors, or whether the observed behaviour, which is apparently chaotic, is due to transients or periodic orbits of high period. A particularly interesting case is that of an *interior crisis* [Robert *et. al.*, 1998; RobertAlligoodOttYorke98] in which there is a large change (*explosion*) in the size of an attractor at certain kinds of homoclinic tangency.

The paper is organised as follows: Most of the notation, concepts and definitions used are introduced in Sec. 2. In Sec. 2.1 we describe homoclinic tangles and trellises, in Sec. 2.2 we recall some of the theory of topological graphs, and in Sec. 2.3 we discuss symbolic dynamics. The relation between dynamics of surface diffeomorphisms and graph maps is described in Sec. 3, and illustrated by Ex. 3.3. In Sec. 4 we give details of a general algorithm for computing efficient graph maps. The use of the algorithm is shown in Ex. 4.2. In Sec. 5 we give a detailed study of the area-preserving Hénon map.

2 Tangles and Symbolic Dynamics

In this section, we first introduce some notation and recall basic facts from the theory of homoclinic tangles, graph maps and symbolic dynamics. Refer to Wiggins [1991] for more details on the notation concerning tangles in two dimensions, and Lind & Marcus [1995] for more information on symbolic dynamics.

2.1 Tangles and trellises

If f is a diffeomorphism with a saddle fixed point p , then the stable and unstable sets of p are smooth curves which we denote W^S and W^U respectively. The pair $W = (W^U, W^S)$ is a *homoclinic tangle* for f . If W^U and W^S intersect at a point other than p , they must intersect infinitely often and have infinite length, hence are impossible to draw, compute or describe combinatorially. Therefore, instead of considering the entirety of the stable and unstable curves, we only consider finite sub-intervals T^U and T^S of W^U and W^S . If T^U and T^S both contain p , we call the pair $T = (T^U, T^S)$ a *trellis* for f . A diagram of a simple trellis is shown in Fig. 1, with T^U drawn in red and T^S in blue.

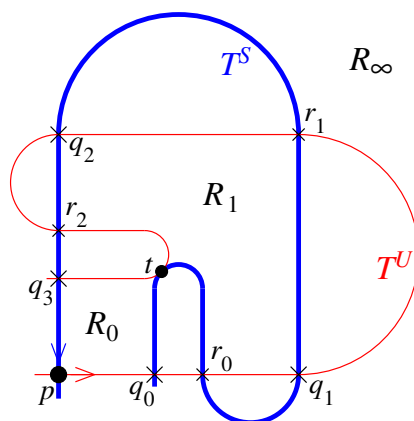


Figure 1: A simple trellis

An *intersection point* is a point in $T^U \cap T^S$. In Fig. 1, the points p , q_0 , q_1 , q_2 , q_3 , r_0 , r_1 , r_2 and t are all intersection points. A trellis is *transverse* if all intersection points are (topologically) transverse crossings of T^U and T^S . The trellis shown is not transverse, since t is a tangential intersection.

The (closed) interval in T^U with endpoints a and b is denoted $T^U[a, b]$, with similar notation for open intervals, and for intervals in T^S . A *segment* is an interval in T^U or

T^S bounded by two intersection points with no other intersection points in its interior. In Fig. 1, $T^U[p, q_0]$ and $T^S[t, q_3]$ are segments, but not $T^S[p, q_0]$. The *ends* of a trellis are the subintervals of T^U and T^S which do not lie in any segment. The ends give no information about the dynamics, and are ignored.

A *primary intersection point* (*pip*) is an intersection point q such that $T^U[p, q] \cup T^S[p, q]$ is a simple closed curve. The points q_0, q_1, q_2, q_3 and r_0, r_1, r_2 are all pips, but t is not, since $T^U[p, t]$ and $T^S[p, t]$ intersect at q_1, q_2, r_0, r_1 and r_2 . We say T is in the n^{th} *Birkhoff signature class* if there is a pip q such that $T^U = T^U[p, f^n(q)]$ and $T^S = T^S[p, q]$. The Birkhoff signature class depends on the diffeomorphism as well as the trellis. If, for the trellis in Fig. 1, we have a diffeomorphism f mapping q_0 to q_1 , we then must have $f^3(q_0) = q_3$, so $T^U = T^U[p, f^3(q_0)]$ and $T^S = T^S[p, q_0]$, and hence the trellis is in the 3rd Birkhoff signature class.

An (open) *region* of T is a component of $\mathbb{R}^2 \setminus (T^U \cup T^S)$. A *closed region* is the closure of an open region, and hence includes the stable and unstable boundary segments. Each region (except for the unbounded region) is a topological disk bounded by (typically alternating) stable and unstable segments. We will denote regions by R_i . The trellis in Fig. 1 has 9 regions, including the unbounded region R_∞ . Region R_0 is bounded by two unstable segments, $T^U[p, q_0]$ and $T^U[t, q_3]$, and two stable segments, $T^S[p, q_3]$ and $T^S[t, q_0]$. Region R_1 is bounded by three unstable segments and three stable segments. All unlabelled regions are bounded by one stable segment and one unstable segment, and are called *lobes*.

2.2 Compatible graphs and graph maps

The topology of a trellis T can be encoded combinatorially by means of a graph. There are many different graphs which represent the same trellis T ; we call all such graphs *compatible* with T . To be compatible with a (planar) trellis T , a graph G must satisfy the following properties:

1. G has two types of edges, *control* edges and *expanding* edges.
2. There is one control edge for each stable segment. This control edge crosses that segment once transversely, but otherwise does not intersect T^U or T^S .
3. Expanding edges do not intersect T^U or T^S .
4. G is connected with no loops. (i.e. G is a tree.)

As described above, a compatible graph is a subset of the plane, and so has a topological structure. The regions of G are the components of $G \setminus T^S$, or equivalently, the restriction of the regions of T to G . Expanding edges lie entirely in one region and control edges straddle two regions.

In this paper, the control edge of a compatible graph intersecting segment S_i will always be denoted z_i . We will always orient the control edge z_i so that if S_i is oriented in the direction of the fixed point p , the pair (S_i, z_i) defines a positive orientation. We denote the expanding edges in a region R_i by a_i, b_i etc. The reverse of an edge e will be denoted \bar{e} , so $\bar{\bar{e}} = e$. The *valence* of a vertex v is n if v has n incident edges. A list $e_1 \dots e_n$ of edges is an *edge-path* if the initial vertex of e_{i+1} is the same as the final vertex of e_i for $1 \leq i < n$. An edge-path $e_1 \dots e_n$ *back-tracks* if $e_{i+1} = \bar{e}_i$ for some i .

We can describe the graph combinatorially by specifying the cyclic ordering of edges incident at each vertex, and remembering which control edge crosses which stable segment. The combinatorics of a compatible graph can be computed using basic techniques of computational geometry. The main reason for representing a trellis combinatorially by a graph is that the corresponding diffeomorphism can be represented by certain maps of the graph which can also be described combinatorially.

If G is a graph, a *graph map* g of G takes a vertex to a vertex, and an edge e from v_1 to v_2 to an edge-path from $g(v_1)$ to $g(v_2)$. Thus graph maps are represented combinatorially, but can be interpreted topologically as mapping e in a piecewise-linear way across its image path.

If f is a diffeomorphism with trellis T , and G is a graph compatible with T , then a graph map g of G is *compatible* with f if the control edge crossing segment S maps to the control edge crossing the segment containing $f(S)$, with orientation the same as f . In other words, if $f(S_i \subset S_j)$, then $g(z_i) = z_j$ if f is orientation-preserving and $g(z_i) = \bar{z}_j$ if f is orientation-reversing. Note that we do not need further conditions on the images of expanding edges. (In the non-planar case there are restrictions on the images of expanding edges.)

In some cases we are not interested in the dynamics on the whole space. If this is the case we can simplify the analysis by only considering an appropriate subgraph \tilde{G} of G . \tilde{G} must be invariant under g (that is, $g(\tilde{G}) \subset \tilde{G}$) and is called an *incomplete compatible graph*.

2.3 Symbolic dynamics

Symbolic dynamics gives us a way of describing the dynamics of a system combinatorially. Given a dynamical system f on a phase space X , we let \mathcal{P} be any finite collection of closed subsets of X . A sequence $\dots P_{i-2}P_{i-1}P_{i_0}P_{i_1}P_{i_2}\dots$ is an *itinerary* of an orbit (x_k) if $x_k \in P_{i_k}$. If f is invertible, we say that $\dots P_{i-2}P_{i-1} \cdot P_{i_0}P_{i_1}P_{i_2}\dots$ is an itinerary of the point x if $f^k(x) \in P_{i_k}$ (and hence is an itinerary of the orbit through x). If f is not invertible, we can still define a *forward itinerary* of a point x , which is a sequence $P_{i_0}P_{i_1}P_{i_2}\dots$ with $f^k(x) \in P_{i_k}$. Note that if sets of \mathcal{P} intersect, a point may have more than one itinerary, and if the sets of \mathcal{P} do not cover X , not all points have an itinerary at all. Typically, sets of \mathcal{P} are chosen to have disjoint interiors, so almost every point of X has a unique (forward) itinerary.

The set of all itineraries of f is the *shift space* of f on \mathcal{P} . \mathcal{P} is the *symbol space* of the shift space. Clearly, if I is an itinerary of a point x , then $f(x)$ has an itinerary $\sigma(I)$, where σ is the shift map

$$\sigma(\dots P_{i-2}P_{i-1} \cdot P_{i_0}P_{i_1}P_{i_2}\dots) = \dots P_{i-1}P_{i_0} \cdot P_{i_1}P_{i_2}P_{i_3}\dots \quad (1)$$

The shift space of f is invariant under σ .

The fundamental problem of symbolic dynamics is to compute the shift space of a map on some given symbol space. Unfortunately, this is often too difficult, so instead, we look for *subshifts* of the shift space of the map. A subshift is a closed subset of the shift space which is invariant under the shift map. We call both the shift space of a map with symbol space \mathcal{P} , and its subshifts, *shifts on \mathcal{P}* .

If f is a diffeomorphism with trellis T , then we take \mathcal{P} to be the set of regions of T . An *itinerary* of a point x is therefore a sequence (R_{i_k}) with $f^k(x) \in R_{i_k}$. A point x has a unique itinerary except for the special case that x is in W^U or W^S .

If g is a controlled graph map compatible with f , we can find the shift space of g on the regions of G . We can also look at the shift space on the expanding edges of g . One particularly nice way of representing this shift is by constructing a directed graph with nodes corresponding to the edges of G , and a directed edge from e_i to e_j for each time g maps e_i across e_j . (In other words, there is one directed edge from e_i to e_j for each time either e_j or \bar{e}_j appears in the edge-path $g(e_i)$.) The itineraries of g correspond to bi-infinite paths in the directed graph. To find the corresponding shift on regions, we simply relabel the node corresponding to the edge e of G by the region R with $e \subset R$. (See Fig. 3 for an example.) Since each expanding edge is contained in a single region of T , we can compute the set of itineraries of g by replacing each edge by the region it lies in. The resulting shift is a *factor* of the shift on expanding edges of G . A shift which is a factor of a finite-type shift is called a *sofic shift*.

We can also represent the dynamics of a graph map g by a *transition matrix* $A = (a_{ij})$ where a_{ij} is the number of times g maps edge e_i across e_j . If A is the transition matrix for g , then A^n is the transition matrix for g^n . There must be one periodic point of g of period n in e_i for each time g^n maps e_i across e_i , so there are $(A^n)_{ii}$ (the i, i^{th} element of A^n) period n points of g in e_i . The topological entropy of g is given by the growth rate of the number of periodic points of g , which is equal to the logarithm of the largest eigenvalue λ_{\max} of A . In other words,

$$h_{\text{top}}(g) = \limsup_{n \rightarrow \infty} \frac{1}{n} \log \text{Tr}(A^n) = \log \lambda_{\max}(A) \quad (2)$$

3 Efficient Graph Maps

Let g be a graph map compatible with f . We have seen that we can find the dynamics of g in terms of a shift on regions of the graph. To find the dynamics of f , we need to relate the dynamics of g to that of f . For most graph maps g compatible with f , there may be itineraries of g which are not itineraries of f , so we need conditions on g under which this cannot occur.

A graph map g of a graph G is *efficient* if

1. The only vertices of G with valence 1 or 2 are the endpoints of a control edge.
2. Any invariant set of edges of G contains a control edge.
3. G is locally one-to-one on the expanding edge set.

Conditions (1) and (2) ensure that the graph G does not have any unnecessary edges. Condition (3) is the crucial condition. It means that each expanding edge maps to an edge-path with no backtracks, and that the images of expanding edges from the same vertex have different initial edges. We write $\mathcal{G}f$ for an efficient graph map compatible with f .

Using a form of *relative Nielsen theory* [Collins, 2001], a topological fixed-point theory, to relate the dynamics of f and g , we can prove the following:

Theorem 3.1 *Let f be a diffeomorphism of \mathbb{R}^2 with connected trellis T , and g be an efficient graph map compatible with f . Then*

1. The shift space of $\mathcal{G}f$ on regions is a subshift of the shift space of f on regions.
2. If I is a periodic itinerary of least period n , then f has a point with itinerary I and least period n .
3. The topological entropy of f is at least that of g

In some special cases, the shift spaces of f and $\mathcal{G}f$ coincide, but in general the shift space of f will be larger than that of $\mathcal{G}f$. This raises the question of whether we could use the information provided by the trellis to find more itineraries. It turns out that we cannot; given any itinerary I not in the shift space of $\mathcal{G}f$, there is a diffeomorphism with trellis T for which I is not an itinerary, and there are diffeomorphisms with trellis T and entropy arbitrarily close to that of $\mathcal{G}f$. We say that the shift space of $\mathcal{G}f$ is the *shift forced by the trellis* T , since it contains all orbits whose existence can be deduced from the trellis.

In many applications, we are interested in how the dynamics of a parameterized family of maps $(f_\lambda)_{\lambda \in \Lambda}$ varies as the parameter is changed. Since stable and unstable manifolds vary smoothly with parameter, the family (f_λ) gives rise to a smoothly varying family of trellises (T_λ) . The topological structure of the T_λ changes only when a trellis has a tangency. Since the shift forced by a trellis depends only on its topology and not its geometry, it too remains unchanged except at tangencies. Of course, the geometry of the regions varies, but does so in a smooth way, giving a natural correspondence between regions of different trellises.

If f is a diffeomorphism with a transverse trellis T , then *any* sufficiently close diffeomorphism has a trellis with the same topological structure as T . By the preceding paragraph, we deduce:

Theorem 3.2 *If f has a transverse trellis T , then the dynamics of f forced by T are present for all sufficiently small perturbations of f .*

This is a very important result, since it implies that the results obtained are meaningful even though the system may not be known exactly, or be subject to numerical errors.

A tangency of stable and unstable curves generically occurs when two homoclinic orbits meet and annihilate each other. This gives a codimension-one bifurcation known as a *homoclinic bifurcation*. While the unfolding of a homoclinic bifurcation is extremely complicated with orbits being both created and annihilated (see, for example, [Guckenheimer & Holmes, 1983]), the entropy *bound* computed from a trellis must decrease as intersection points are removed. The shift forced by the trellis after the bifurcation is, in fact, a subshift of a factor of the shift before the bifurcation. The entropy need not *strictly* decrease; in many cases there are four homoclinic orbits with the same topological type which are removed in pairs, and typically the entropy only decreases strictly when the second pair is removed.

Example 3.3

The Hénon map

$$(x, y) \mapsto (a - x^2 - by, x) \tag{3}$$

with parameter values $a = \frac{3}{2}$ and $b = \frac{4}{5}$ has a trellis T_3 shown in Fig. 2 together with a compatible graph g . The hyperbolic saddle fixed point is marked with a dot, and four pips on the same orbit are marked with crosses (+). Control edges of g are thick green lines with solid arrows; expanding edges are thin black lines. Note that this graph is incomplete, since not all stable segments are crossed by control edges.

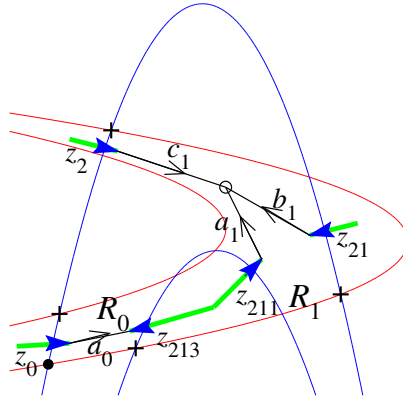


Figure 2: Trellis with compatible graph

In a compatible graph map, the control edges $z_0, z_2, z_{21}, z_{211}$ and z_{213} map

$$z_{213}, z_{211} \mapsto z_{21} \mapsto z_2 \mapsto z_0 \mapsto z_0 \quad (4)$$

(Note that the control edges are labelled so the image of a control edge can be found by removing the last digit of the label.) Further, if the expanding edges map

$$a_0 \mapsto a_0 \bar{z}_{213} z_{211} a_1 \bar{b}_1, \quad a_1 \mapsto b_1, \quad b_1 \mapsto c_1, \quad c_1 \mapsto a_0 \bar{z}_{213} z_{211} a_1 \quad (5)$$

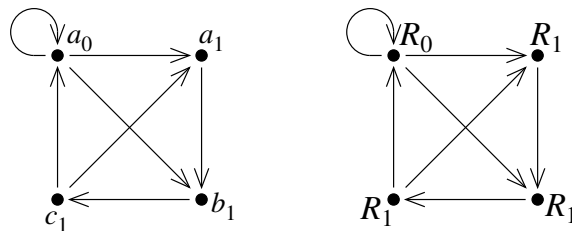
then the resulting map is efficient, since none of the edge images back-track, and the map is also injective near the valence-3 vertex.

The transition matrix is

$$A = \begin{pmatrix} & a_0 & a_1 & b_1 & c_1 \\ a_0 & 1 & 1 & 1 & 0 \\ a_1 & 0 & 0 & 1 & 0 \\ b_1 & 0 & 0 & 0 & 1 \\ c_1 & 1 & 1 & 0 & 0 \end{pmatrix} \quad (6)$$

which has characteristic polynomial $\lambda(\lambda^3 - \lambda^2 - 2)$, so the topological entropy of the graph map is $\log \lambda_{\max}$, where λ_{\max} is the largest root of the equation $\lambda^3 - \lambda^2 - 2 = 0$. Numerically, $\lambda_{\max} \approx 1.70$, so $h_{\text{top}}(f) \geq 0.527$.

The shift map for g is given by the directed graph shown in Fig. 3(a). Replacing edge a_0 with its region R_0 , and edges a_1, b_1 and c_1 with R_1 we obtain the shift for f , which is shown in Fig. 3(b).


 Figure 3: (a) Shift on edges for g . (b) Shift on regions for f .

We can now read off the itineraries forced by T . The only itineraries which need not be present in f are those which contain sub-words of the form $R_0R_1^{3n-2}R_0$ for $n \in \mathbb{N}$. Thus, for example, periodic orbits with itineraries $(R_0R_1R_1)^\infty = \dots R_0R_1R_1R_0R_1R_1R_0\dots$ and $(R_0R_1R_1R_1)^\infty$ must be present in f , but periodic orbits with itineraries $(R_0R_1)^\infty$ or $(R_0R_1R_1R_1R_1)^\infty$ need not be, since these contain the words $R_0R_1^1R_0$ and $R_0R_1^4R_0$ respectively. Likewise, there must be a homoclinic orbit with itinerary $R_0^\infty R_1R_1R_0^\infty = \dots R_0R_0R_1R_1R_0R_0\dots$ but not necessarily $R_0^\infty R_1R_0R_1R_0^\infty$.

4 Computing an Efficient Compatible Graph Map

In many cases, an efficient graph map compatible with a diffeomorphism f with trellis T can be found by inspection. To be able to deal with more complicated cases, we present the following algorithm.

Algorithm 4.1 A efficient compatible graph map can be obtained as follows: First construct a compatible map.

1. Draw one control edge for each stable segment. Each region with n stable segments on its boundary now contains n vertices, each at the end of a control edge.
2. For each region with n stable segments on its boundary, join the n vertices with $n - 1$ expanding edges.
3. The image of each control edge is determined by the image of the stable segment it crosses. Since all vertices are endpoints of control edges, their images are then known. If e is an expanding edge from v_1 to v_2 , we take $g(e)$ to be the unique edge-path from $g(v_1)$ to $g(v_2)$ which does not backtrack.

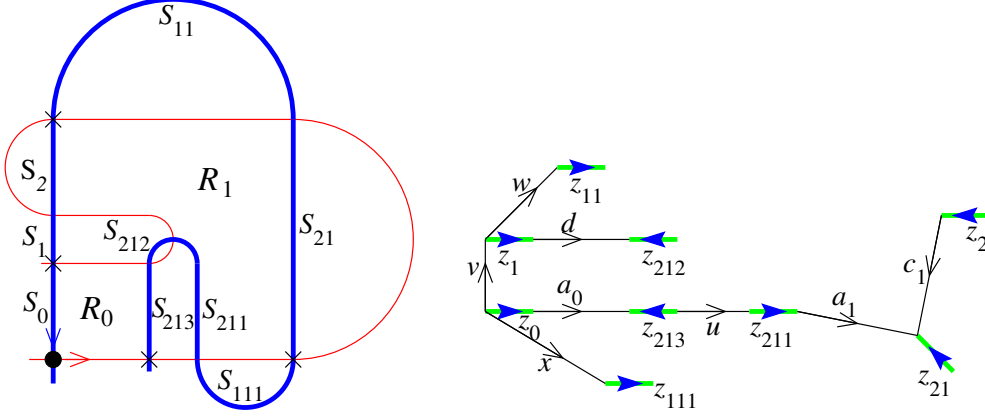
Now perform the following moves until the graph is efficient.

4. If there is an invariant set of edges of G which does not contain a control edge, collapse each of these edges to points.
5. If the image of an edge back-tracks, homotope to remove this. In other words, if $g(e) = \epsilon_0 e_1 \bar{e}_1 \epsilon_2$, then $g'(e) = \epsilon_0 \epsilon_2$, where g' is the new graph map.
6. If there is a valence-3 vertex v with incident edges e_1 , e_2 and e_3 , each of which is expanding, such that $g(e_1)$ and $g(e_2)$ have the same initial edge-path ϵ_0 homotope so that $g'(v)$ moves to the other end of ϵ_0 . In other words, if $g(e_1) = \epsilon_0 \epsilon_1$, $g(e_2) = \epsilon_0 \epsilon_2$ and $g(e_3) = \epsilon_3$, then $g'(e_1) = \epsilon_1$, $g'(e_2) = \epsilon_2$ and $g'(e_3) = \bar{\epsilon}_0 \epsilon_3$, where g' is the new graph map.
7. If there is a vertex v with expanding edges e_1 and e_2 such that $g(e_1)$ and $g(e_2)$ have the same initial edge-path, *fold* the initial pieces of e_1 and e_2 together to obtain new edges e'_0 , e'_1 and e'_2 with $e_1 = e'_0 e'_1$, $e_2 = e'_0 e'_2$ and $g(e'_0) = \cdot$. Now remove back-tracks, if possible, as in (5), homotope as in (6) and collapse invariant edges if necessary as in (4).

This algorithm is a modification of the Bestvina-Handel algorithm for periodic orbits [Bestvina & Handel, 1995]. It is guaranteed to terminate.

Example 4.2

We now show how the efficient graph map compatible with the trellis T_3 of Ex. 3.3 could have been computed using the above algorithm. The trellis and an initial compatible graph (constructed using steps (1) and (2) of the algorithm) are shown in Fig. 4.


 Figure 4: Trellis T_3 and initial compatible graph

The control edges map under g as follows:

$$z_0, z_1, z_2 \mapsto z_0, \quad z_{11} \mapsto z_1, \quad z_{21} \mapsto z_2, \quad z_{111} \mapsto z_{11}, \quad z_{211}, z_{212}, z_{213} \mapsto z_{21} \quad (7)$$

Using step (3) we can compute g on the expanding edges, which map:

$$\begin{aligned} a_0, d \mapsto a_0 \bar{z}_{213} u z_{211} b_1, \quad a_1 \mapsto \bar{c}_1, \quad c_1 \mapsto a_0 \bar{z}_{213} u z_{211} a_1 \bar{c}_1 \\ u \mapsto \cdot, \quad v \mapsto \cdot, \quad w \mapsto v, \quad x \mapsto vw \end{aligned} \quad (8)$$

The edges u , v , w and x form an invariant subset which does not contain any control edges. By step (4) of the algorithm, each of these edges can be collapsed to a point to give the graph in Fig. 5.

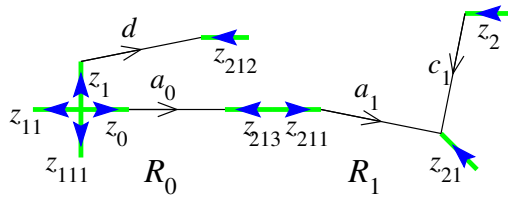


Figure 5: Graph obtained by collapsing invariant set

The expanding edges a_0 , a_1 , c_1 and d map:

$$a_0, d \mapsto a_0 \bar{z}_{213} z_{211} b_1, \quad a_1 \mapsto \bar{c}_1, \quad c_1 \mapsto a_0 \bar{z}_{213} z_{211} a_1 \bar{c}_1 \quad (9)$$

The edges a_1 and c_1 map to a edge-paths with the same final edge \bar{c}_1 so we fold them together as in step (7) to form edges a'_1 , b'_1 and c'_1 where $a_1 = a'_1 \bar{b}'_1$ and $c_1 = c'_1 \bar{b}'_1$, as shown in Fig. 6.

The new graph map g' is

$$a_0, d \mapsto a_0 \bar{z}_{213} z_{211} a'_1 \bar{b}'_1, \quad a'_1 \mapsto b'_1 \bar{c}'_1, \quad b'_1 \mapsto \cdot, \quad c_1 \mapsto a_0 \bar{z}_{213} z_{211} a'_1 \bar{b}'_1 b'_1 \bar{c}'_1 \quad (10)$$

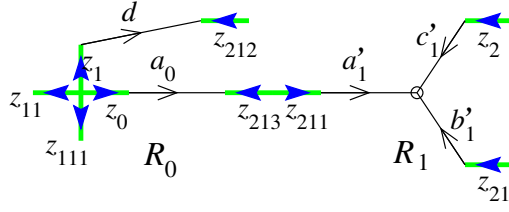


Figure 6: Graph after folding

We see that the image of c'_1 back-tracks, which we remove by a homotopy as in step (5) so that $c'_1 \mapsto a_0 \bar{z}_{213} z_{211} a'_1 \bar{c}'_1$. Since now each of a'_1 , b'_1 and c'_1 are expanding, we can homotope as by step (6) so that

$$a'_1 \mapsto b'_1, \quad b'_1 \mapsto c'_1, \quad c'_1 \mapsto a_0 \bar{z}_{213} z_{211} a'_1 \quad (11)$$

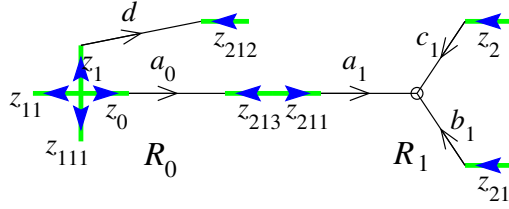


Figure 7: Final graph

Dropping the primes, we obtain the graph in Fig. 7 and an efficient graph map

$$a_0, d \mapsto a_0 \bar{z}_{213} z_{211} a_1 \bar{b}_1, \quad a_1 \mapsto b_1, \quad b_1 \mapsto c_1, \quad c_1 \mapsto a_0 \bar{z}_{213} z_{211} a_1 \quad (12)$$

which is the same as originally given in Ex. 3.3.

5 Trellises and Bifurcations in the Hénon Family

As an illustration of our methods, we have computed trellises, compatible tight graph maps and entropy bounds for the area-preserving Hénon map

$$(x, y) \mapsto (a - x^2 - y, x) \quad (13)$$

as the parameter a decreases from 5.65 to 2.20. All trellises have been computed to the 5th Birkhoff signature class. The graphs given are incomplete, but contain all the chaotic dynamics. The reader is encouraged to reproduce the calculation of the graph maps and entropy bounds from the trellis.

Most control edges have been labelled in pairs. Following our standard notation, the edges of the graphs have been labelled so that expanding edges with the same subscript lie in the same region. Expanding edges with the same letter lie on the same edge-path, and the image of this path is given in terms of other edge-paths. For simplicity, we drop the control edges in these edge-paths. For example, in Example (b), b denotes the edge-path $b_4 b_3$, $e = e_5$ and $f = f_8 f_7 f_6$ (where we ignore control edges). Since $b_3 \mapsto f_6 \bar{e}_5$ and $b_4 \mapsto f_8 f_7$, we find $b = b_4 b_3 \mapsto f_8 f_7 f_6 \bar{e}_5 = f \bar{e}$

In the parameter range under consideration, there are nine topologically inequivalent transverse trellises. Trellis H_0 is topologically equivalent to a trellis for the Smale horseshoe map [Guckenheimer & Holmes, 1983]. The other trellises occur in pairs with the same entropy. Of these pairs we have only given graphs maps for the trellis with the fewest intersection points. Notice how no new intersection points are created as a is decreased, and each time intersection points are removed the entropy does not increase.

For the relatively simple trellises considered here, it is practical to compute the dynamics by hand. In more complicated cases, hand computations are long, tedious and error-prone, and a computer implementation is required.

Acknowledgements

The author would like to thank Bernd Krauskopf for a careful reading of the manuscript and many suggestions for improving the exposition, and Morris Hirsch and Toby Hall for their help and support.

This work was partially funded by Leverhulme Special Research Fellowship SRF/4/9900172.

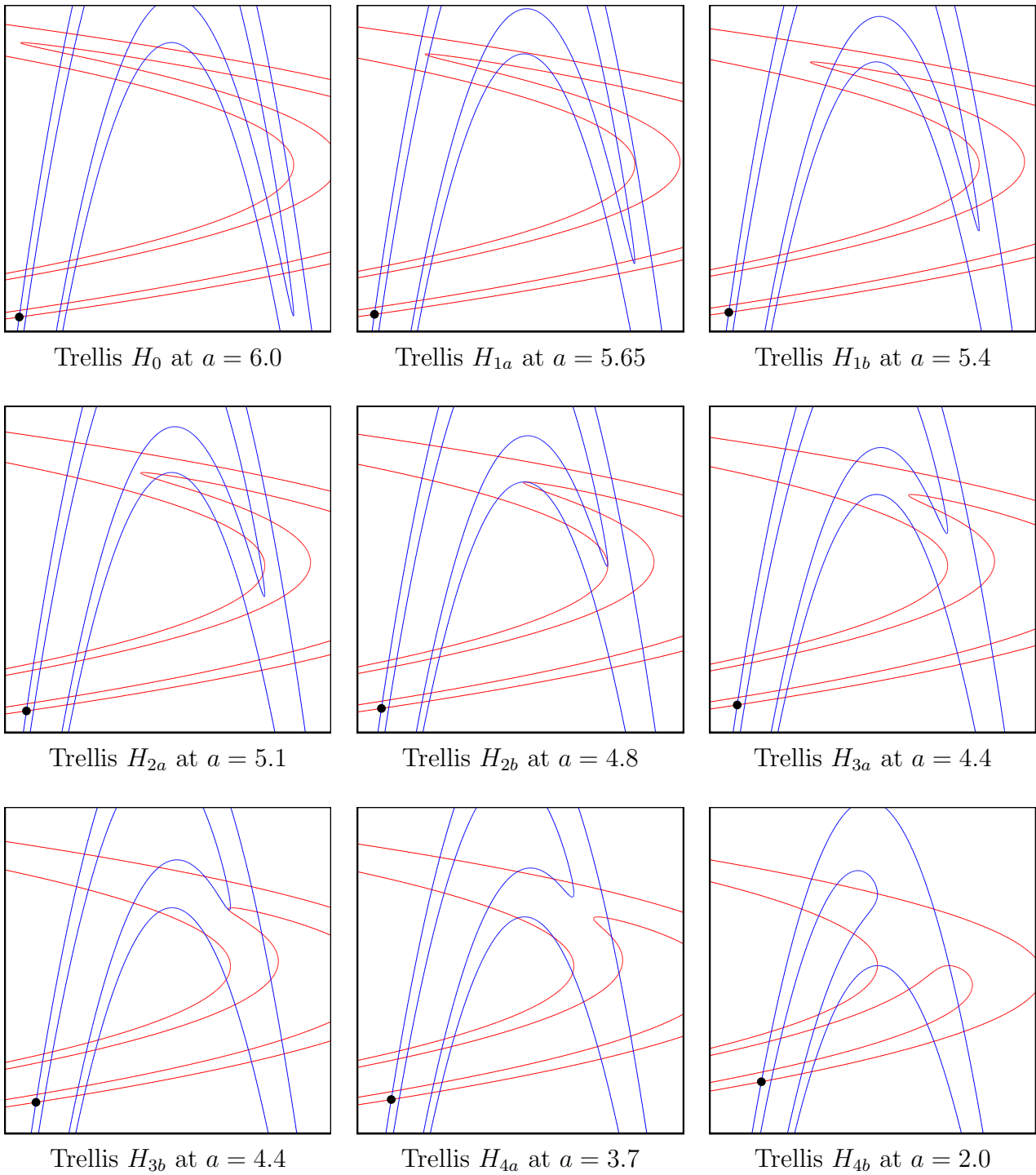


Figure 8: Trellises in the area-preserving Hénon map.

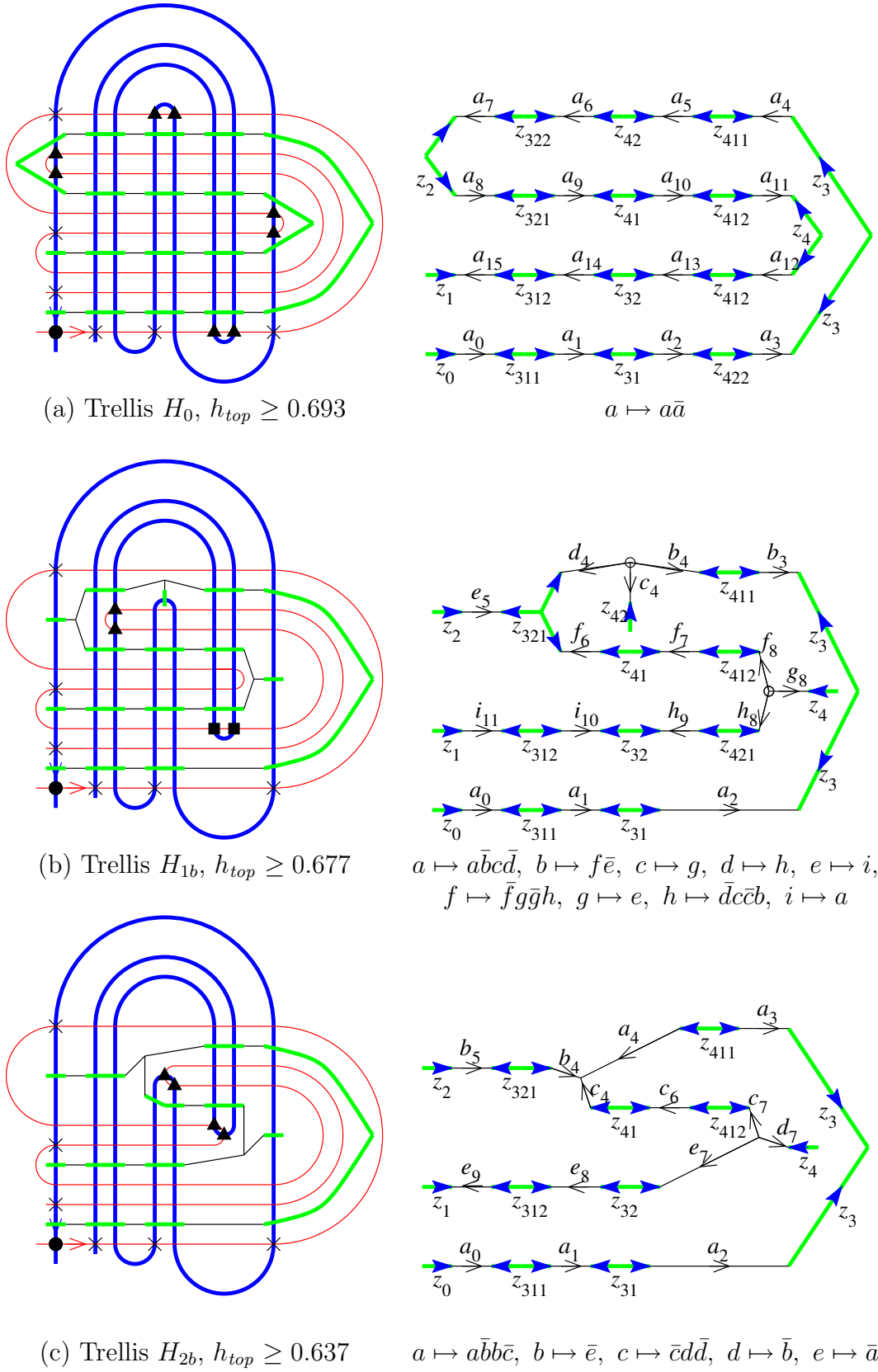


Figure 9: Trellises and graphs for the area-preserving Hénon map. (a) — (c)

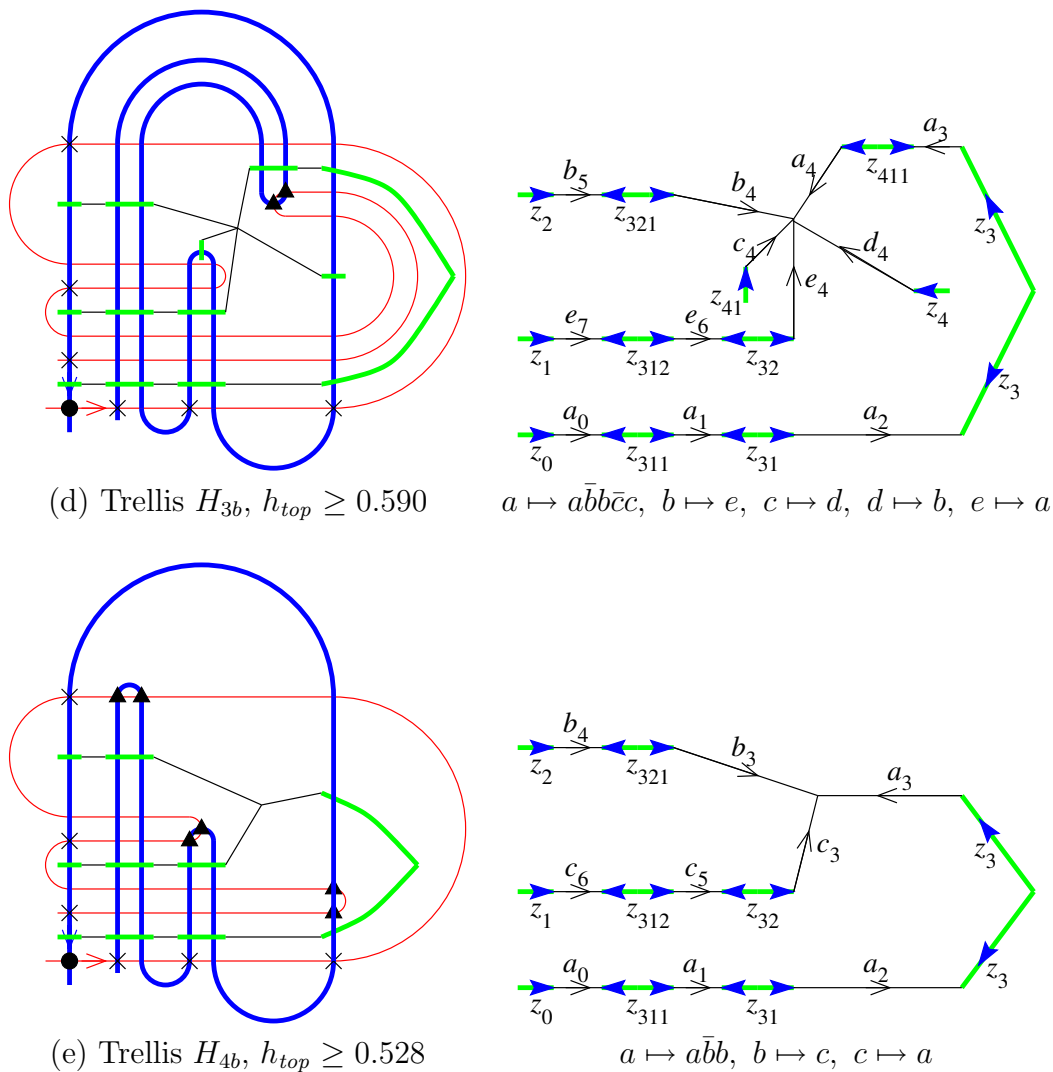


Figure 9: Trellises and graphs for the area-preserving Hénon map. (d) — (e)

References

- Back, A. & Guckenheimer, J. & Meyers, M. R. & Wicklin, F. J. & Worfolk P.A. [1992] “DsTool: computer assisted exploration of dynamical systems,” *Notices Amer. Math. Soc.* **39**, 303.
- Bestvina, M. & Handel, M. [1995] “Train-tracks for surface homeomorphisms” *Topology* **34**(1), 109–140.
- Beyn, W. J. & Kleinkauf, J. M. [1997] “The numerical computation of homoclinic orbits for maps,” *SIAM J. Numer. Anal.* **34**(3) 1207–1236.
- Boyland, P. L. & Aref, H. & Stremler, M. A. [2000] “Topological fluid mechanics of stirring,” *J. Fluid Mech.* **403** 277–304.
- Collins, P. J. [1999a] “Dynamics forced by surface trellises,” in *Geometry and Topology in Dynamics*, eds. Barge, M. & Kuperberg, K. (American Mathematical Society, Providence, R.I.) pp. 65–86.
- Collins, P. J. [1999b] “Diffeomorphisms with Homoclinic and Heteroclinic Tangles,” *PhD thesis*, (University of California, Berkeley).
- Collins, P. J. [2001] “Relative periodic point theory,” *Topology Appl.* **115**(1) 97–114.
- Conley, C. [1978] *Isolated Invariant Sets and the Morse Index* (American Mathematical Society, Providence, R.I.).
- Davidchack, R. L. & Lai, Y.-C. [1999] “Efficient algorithm for detecting unstable periodic orbits in chaotic systems,” *Phys. Rev. E.* **60**(5), 6172–6175.
- Franks, J. & Misiurewicz, M. [1993] “Cycles for disk homeomorphisms and thick trees,” in *Nielsen Theory and Dynamical Systems*, (American Mathematical Society, Providence, R.I.) pp. 69–139.
- Guckenheimer, J. & Holmes, P. [1983] *Nonlinear Oscillations, Dynamical Systems, and Bifurcations of Vector Fields*. (Springer-Verlag, Berlin).
- Handel, M. [1999] “A fixed-point theorem for planar homeomorphisms,” *Topology* **38**(2), 235–264.
- Hansen, K. [1995] “Alternative method to find orbits in chaotic systems,” *Phys. Rev. E* **52**(3), 2388–2391.
- Hobson, D. [1993] “An efficient method for computing invariant manifolds of planar maps,” *J. Comput. Phys.* **104**(1), 14–22.
- Homburg, A. J. & Osinga, H. & Vegter, G. [1995] “On the computation of invariant manifolds of fixed points,” *Z. Angew. Math. Phys.* **46**(2), 171–187.
- Hulme, H. [2000] “Finite and infinite braids: a dynamical systems approach,” *PhD thesis*, (University of Liverpool).
- Jiang, B. [1983] *Lectures on Nielsen Fixed Point Theory*. (American Mathematical Society, Providence, R.I.).

Krauskopf, B. & Osinga, H. [1998] “Growing 1d and quasi-2d unstable manifolds of maps,” *J. Comput. Phys.* **146**(1), 404–419.

Lind, D. & Marcus, B. [1995] *An Introduction to Symbolic Dynamics and Coding*. (Cambridge University Press).

McRobie, F. A. & Thompson, J. M. T. [1993] “Driven oscillators, knots, braids and Nielsen-Thurston theory,” in *Nonlinearity and Chaos in Engineering Dynamics*, eds. Thompson J. M. T. & Bishop, S. R. (Wiley, Chichester), pp. 317–328.

McRobie, F. A. & Thompson, J. M. T. [1994] “Knot-types and bifurcations sequences of homoclinic and transient orbits of a single-degree-of-freedom driven oscillator,” *Dynam. Stab. Sys.* **9**, 223–251.

Mischaikow, K. [1997] “Conley index theory,” in *Dynamical Systems*, ed. Johnson, R. (Springer, Berlin) pp. 119–207.

Mischaikow K. & Mrozek, M. [1995] “Chaos in the Lorentz equations: a computer assisted proof,” *Bull. Amer. Math. Soc. (N.S.)* **33** 66–72.

Mischaikow, K. & Mrozek, M. & Reiss, J. & Szymczak, A. [1999] “Construction of symbolic dynamics from experimental time series,” *Phys. Rev. Lett.* **82**(6) 1144–1147.

Palis, J. & Takens, F. [1993] *Hyperbolicity and sensitive chaotic dynamics at homoclinic bifurcations*. (Cambridge University Press).

Parker, T. & Chua, L. [1989] *Practical Numerical Algorithms for Chaotic Systems*. (Springer Verlag, Berlin).

Robert, C. & Alligood, K. & Ott, E. & Yorke, J. A. [1998] “Outer tangency bifurcations of chaotic sets,” *Phys. Rev. Lett.* **80**(22), 4867–4870.

Rom-Kedar, V. [1994] “Homoclinic tangles—classification and applications,” *Nonlinearity* **7**(2), 441–473.

Schmelcher, P. & Diakonov, F. K. [1998] “General approach to the localization of unstable periodic orbits in chaotic dynamical systems,” *Phys. Rev. E* **57**(3), 2739–2746.

Simó, C. [1989] On the analytical and numerical approximation of invariant manifolds. in *Les Méthodes Modernes de la Mécanique Céleste*, eds. Benest, D. & Froeschlé, C. pp. 285–329.

Solari, H. G. & Natiello, M. A. & Vázquez, M. [1996] “Braids on the Poincaré section: a laser experiment,” *Phys. Rev. E* **54**(4), 3185–3195.

Thurston, W. P. [1988] “On the geometry and dynamics of diffeomorphisms of surfaces,” *Bull. Amer. Math. Soc. (N.S.)* **19**(2), 417–431.

Wang, Q. & Young, L.-S. [1999] “Analysis of a class of strange attractors,” *Preprint*.

Wiggins, S. [1991] *Chaotic Transport in Dynamical Systems*. (Springer-Verlag, Berlin).

You, Z. & Kostelich, E. J. & Yorke, J. A. [1991] “Calculating stable and unstable manifolds,” *Intern. J. Bifur. Chaos* **1**(3), 605–623.